





RESEARCH ARTICLE

Physiological instability is linked to mortality in primary central nervous system lymphoma: A case–control fMRI study

Valter Poltoja ^{1,2,3}  | Janette Kempainen ^{1,4} | Nina Keinänen ⁵ |
 Michaela Bode ^{2,3} | Juha-Matti Isokangas ³ | Hanne Kuitunen ⁶ | Juha Nikkinen ^{2,7} |
 Eila Sonkajärvi ⁵ | Vesa Korhonen ^{1,2,3} | Timo Tuovinen ^{1,2,3} | Matti Järvelä ^{1,2,3} |
 Niko Huotari ^{1,2,3} | Lauri Raitamaa ^{1,2,3}  | Janne Kananen ^{1,2,3}  |
 Tommi Korhonen ^{8,9} | Sami Tetri ^{8,9} | Outi Kuittinen ^{6,10,11} | Vesa Kiviniemi ^{1,2,3} 

¹Oulu Functional Neuroimaging, University of Oulu/Oulu University Hospital, Oulu, Finland

²Medical Imaging, Physics and Technology, University of Oulu, Oulu, Finland

³Department of Radiology, Oulu University Hospital, Oulu, Finland

⁴Cancer and Translational Medicine Research Unit, University of Oulu, Oulu, Finland

⁵Department of Anaesthesiology, Oulu University Hospital, Oulu, Finland

⁶Department of Oncology and Haematology, Oulu University Hospital, Oulu, Finland

⁷Department of Oncology and Radiotherapy, Oulu University Hospital, Oulu, Finland

⁸Medical Research Center, University of Oulu/Oulu University Hospital, Oulu, Finland

⁹Department of Clinical Neuroscience, University of Oulu, Oulu, Finland

¹⁰Cancer Center, Kuopio University Hospital, Kuopio, Finland

¹¹Faculty of Health Medicine, Institute of Clinical Medicine, University of Eastern Finland, Oulu, Finland

Correspondence

Vesa Kiviniemi, Department of Diagnostic Radiology, P.O. Box 50, 90029 OYS, Oulu, Finland.

Email: vesa.kiviniemi@oulu.fi

Funding information

Academy of Finland, Grant/Award Numbers: Project 338599, TERVA 314497, TERVA 335720; Instrumentarium Science Foundation (Janne Kananen); Jane ja Aatos Erkko Foundation; Maire Taponen Foundation (Janne Kananen); Medical Research Center Oulu

Abstract

Primary central nervous system lymphoma (PCNSL) is an aggressive brain disease where lymphocytes invade along perivascular spaces of arteries and veins. The invasion markedly changes (peri)vascular structures but its effect on physiological brain pulsations has not been previously studied. Using physiological magnetic resonance encephalography (MREG_{BOLD}) scanning, this study aims to quantify the extent to which (peri)vascular PCNSL involvement alters the stability of physiological brain pulsations mediated by cerebral vasculature. Clinical implications and relevance were explored. In this study, 21 PCNSL patients (median 67y; 38% females) and 30 healthy age-matched controls (median 63y; 73% females) were scanned for MREG_{BOLD} signal during 2018–2021. Motion effects were removed. Voxel-by-voxel Coefficient of Variation (CV) maps of MREG_{BOLD} signal was calculated to examine the stability of physiological brain pulsations. Group-level differences in CV were examined using nonparametric covariate-adjusted tests. Subject-level CV alterations were examined against control population Z-score maps wherein clusters of increased CV values were detected. Spatial distributions of clusters and findings from routine clinical neuroimaging were compared [contrast-enhanced, diffusion-weighted, fluid-attenuated inversion recovery (FLAIR) data]. Whole-brain mean CV was linked to short-term mortality with 100% sensitivity and 100% specificity, as all deceased patients revealed higher values ($n = 5$, median 0.055) than surviving patients ($n = 16$, median 0.028) ($p < .0001$). After adjusting for medication, head motion, and age, patients revealed higher CV values (group median 0.035) than healthy controls (group median 0.024) around arterial territories ($p \leq .001$). Abnormal clusters (median $1.10 \times 10^5 \text{mm}^3$) extended spatially beyond FLAIR lesions (median $0.62 \times 10^5 \text{mm}^3$) with differences in volumes ($p = .0055$).

This is an open access article under the terms of the [Creative Commons Attribution-NonCommercial-NoDerivs](https://creativecommons.org/licenses/by-nc-nd/4.0/) License, which permits use and distribution in any medium, provided the original work is properly cited, the use is non-commercial and no modifications or adaptations are made.

© 2022 The Authors. *Human Brain Mapping* published by Wiley Periodicals LLC.

(Janne Kananen); Orion Research Foundation (Janette Kempainen); Finnish Brain Foundation (Janne Kananen); Finnish Medical Foundation (Janne Kananen, Timo Tuovinen, Janette Kempainen)

KEYWORDS

brain pulsation, functional imaging, lymphoma, malignancy, mortality

1 | INTRODUCTION

Primary central nervous system lymphoma (PCNSL) is a rare group of lymphomas confined to the central nervous system, most commonly B-cell lymphoma. PCNSL has a diffuse, whole brain invasion pattern that results in aggressive disease progression. Most patients develop neurological symptoms within weeks, such as focal deficits, behavioural changes, cognitive impairment, headaches, and vomiting (Grommes & DeAngelis, 2017). While some treatment options have long resulted in unfavourable prognosis in this rapidly progressing malignancy, promising and safe treatment options are emerging with effective curative responses (Angelov et al., 2009; Kuitunen et al., 2017). Regardless of therapeutic advances, there are no simple prognostic biomarkers for PCNSL that may be used, for example, when selecting patients for advanced therapy. Indeed, previous prognostic multivariate models have not produced precise and simple cut-off values but rather have included serum and cerebrospinal fluid (CSF) analytics, age, performance scores, involvement of deep brain structures in diagnostic MRI, histological staining, and genetic profiling (Angelov et al., 2009; Ferreri et al., 2003; Niparuck et al., 2019).

In diagnostic MRI, about 95% of PCNSL cases show moderate to intense homogenous contrast enhancement joined with a larger perilesional T2-weighted fluid-attenuated inversion recovery (FLAIR) hyperintensity. Restricted diffusion is present in 72% of PCNSL cases and may differentiate PCNSL from other malignancies (Cheng & Zhang, 2019; Grommes & DeAngelis, 2017; Haldorsen et al., 2009; Küker et al., 2005; Mansour et al., 2014). However, still some 25% of cases may present atypical imaging patterns (Lin et al., 2020). Limited data from MR-spectroscopy and PET-imaging reveals aberrant metabolism beyond contrast-enhancing areas (Cheng & Zhang, 2019; Küker et al., 2005; Mansour et al., 2014).

A notable radiological shortcoming is the inability to detect the microscopic PCNSL invasion behind radiologically intact blood-brain barrier (BBB). Some 80% of PCNSL relapses occur in spatially distinct locations from the initial contrast-enhancing focus where the BBB is leaking, and therefore CSF-mediated seeding from radiologically occult areas has been proposed (Ambady et al., 2017). Ultrastructural evidence from biopsies shows that invasion of malignant lymphocytes in PCNSL causes loss of small capillaries and extensive structural (peri)vascular alterations with respect to variable endothelial cell thickness, variable basement membrane thickness, endothelial discontinuation, and astrocyte reactions (Aho et al., 1993; Molnár et al., 1999; O'Connor et al., 2019). Elsewhere, malignant lymphocytes invade along enlarged perivascular spaces in angiocentric, sleeve-like extensions behind an intact BBB (Aho et al., 1993; Ambady et al., 2017).

While noninvasive physiological brain imaging has recently raised increasing interest, the *in vivo* physiology of brain tumours has not

been extensively studied. In this respect, it was recently shown with fMRI that beta-amyloid depositions that invade (peri)vascular structures in Alzheimer's disease affect magnetic resonance encephalography (MREG_{BOLD}) signal as a sign of altered cerebrovascular brain pulsations even in radiologically preserved brain areas (Rajna et al., 2021; Tuovinen et al., 2020). Indeed, since cerebrovascular pulsations are known to drive blood flow and perivascular CSF flow (Iliff et al., 2013; Mestre et al., 2018; Rasmussen et al., 2018) and since physiological pulsations stem from blood vessels and from CSF, the T2*-weighted MREG_{BOLD} sequence may detect aberrant cerebrovascular pulsation in multiple compartments of the brain (Assländer et al., 2013; Hennig et al., 2021; Huotari et al., 2019; Kiviniemi et al., 2016; Raitamaa et al., 2021). Moreover, the joined stability of all physiological signal components can be quantified with Coefficient of Variation (CV) that has been found sensitive in detecting unstable brain pulsation even in otherwise radiologically intact brain regions (Kananen et al., 2018, 2020; Tuovinen et al., 2020). Previously blood oxygen level-dependent fMRI signal CV has been linked to physiological stability and (peri)vascular properties such as (neuro)vascular degeneration, cerebrovascular reactivity, CSF flow, and cerebral blood volume (Jahanian et al., 2014; Kananen et al., 2018, 2020; Makedonov et al., 2013, 2016). Since previous studies have documented some similar (peri)vascular properties in PCNSL, MREG_{BOLD} signal CV offers a method for detecting physiological alterations in PCNSL brain.

Based on previous physiological imaging data, we hypothesized that the documented (peri)vascular lymphocyte invasion in PCNSL affects the stability of physiological pulsations that could be measured using MREG_{BOLD} signal CV. We further hypothesized that CV changes extend beyond tissue FLAIR hyperintensities which are currently regarded as the most sensitive diagnostic feature in PCNSL. Finally, we evaluated the link between whole brain mean CV and mortality in PCNSL patients who are treated with blood-brain barrier disruption (BBBD) augmented therapy that has shown promising results (Angelov et al., 2009; Kuitunen et al., 2017).

2 | MATERIALS AND METHODS

2.1 | Subjects and Ethics

In this retrospective case-control study, we consecutively enrolled 40 subjects with known or suspected PCNSL. Fifteen suspects were excluded due to histopathological diagnosis (glioma, haematoma, etc.), one PCNSL patient was excluded due to excessive supra voxel-scale motion, and three PCNSL patients due to scanning at late treatment phase. Final analysis included 21 pathologically confirmed PCNSL patients [median 67y, females 8/21 (38%)] and 30 age-matched

healthy controls [median 63y, females 22/30 (73%)]. Compliant with the standardized BBBB-protocol, the five-drug induction regimen included rituximab, methotrexate, carboplatin, cyclophosphamide, and etoposide (Angelov et al., 2009; Kuitunen et al., 2017). Treatment was given with 3–4-week intervals. Autologous stem-cell transplantation with high-dose chemotherapy was given as consolidation. Seventeen patients received BBBB treatment with curative intent. Four relapsed patients did not receive BBBB treatment since two were ineligible for curative therapy and two did not receive timely intervention due to rapid disease progression.

Pre-defined recruitment criteria for healthy controls included self-reported health and absence of structural brain lesions. However, due to the control population's age, blood pressure medication was allowed for recruitment purposes. Controls' structural MRI data was examined by a neuroradiologist. From 66 enrolled control subjects, two were excluded due to incidental MRI findings. Age-matching was achieved with 30 control subjects. None of the included control subjects were suspected of having neurodegenerative disorders. This study adheres to the Declaration of Helsinki and institutional approval was granted by the Ethical Committee of Northern Ostrobothnia Hospital District. Written informed consent was obtained from all subjects. Data was gathered between May 2018 and May 2021.

2.2 | Scanning

Functional MRI was performed using a MAGNETOM Skyra 3 T 32-channel head coil (Siemens Healthineers AG, Munich, Germany) and a magnetic resonance encephalography (MREG_{BOLD}) sequence: TR 100 ms, TE 36 ms, FA 25°, 5 min scan, isotropic voxel 3 mm. MREG_{BOLD} acquires the entire brain volume with single excitation, and fast imaging is based on undersampling the k-space with a stack-of-spirals trajectory, parallel multi-coil imaging, and regularized image reconstruction (Assländer et al., 2013; Hennig et al., 2021). Image reconstruction was based on L2-Tikhonov regularization (Hugger et al., 2011; Huotari et al., 2019). Due to high temporal resolution of MREG_{BOLD}, physiological signal components may be precisely identified without aliasing (Huotari et al., 2019; Kiviniemi et al., 2016; Raitamaa et al., 2021; Rajna et al., 2021).

High-resolution T1-weighted 3D-MPRAGE data was obtained during the same session (Table S1). During the same session, heart rate was monitored using a finger plethysmograph and respiration rate was monitored using a respiration belt. Additionally, patients were scanned for clinical imaging data: fluid-attenuated inversion recovery (FLAIR), diffusion-weighted, and T1-weighted contrast-enhanced imaging (Table S1). Five FLAIR datasets were obtained 3 days before MREG_{BOLD} acquisition using standard imaging parameters on other scanners.

2.3 | Pre-processing

MREG_{BOLD} and 3D-MPRAGE data were pre-processed using FSL 5.0.9 pipelines (FMRIB, Oxford, UK) (Jenkinson et al., 2012).

T1-relaxation effects were minimized by deleting first 18 s (180 timepoints) from MREG_{BOLD} data, and timeseries were high-pass filtered at 0.008 Hz. MREG_{BOLD} and 3D-MPRAGE data were brain-extracted with neck clean-up and biased field correction. Head motion effects were removed using MCFLIRT software. MREG_{BOLD} data were spatially smoothed with a 5 mm Gaussian kernel and registered to respective 3D-MPRAGE data. MREG_{BOLD} timeseries and their corresponding spatial maps were extracted, and Gaussian noise was filtered with MELODIC ICA. Finally, *3dDespike* was applied to MREG_{BOLD} data to further minimize motion artefacts. Further calculations were performed using FSL, AFNI 20.1.2018 (NIH, Maryland, USA), LIPSIA 3.1.0 (Lohmann et al., 2018) and Prism 9.1.0 (GraphPad, San Diego, USA) software.

Scan-specific absolute and relative head displacement values were collected from MCFLIRT reports. Absolute displacement measures the mean amount of head movement in relation to a reference volume while relative displacement measures the mean amount of head movement in relation to the following volume. Moreover, scan-specific framewise displacement values were calculated to index the joined effects of translational and rotational head displacement, or the amount of head movement between consecutive volumes (Power et al., 2014). More specifically, framewise head displacement is calculated as the absolute sum of three translation length derivatives and three rotation length derivatives. Before summation, the three temporal derivatives of rotation angles are transformed to arc length using a sphere with a 50 mm radius.

2.4 | Calculating CV maps

Coefficient of Variation (CV) was calculated to quantify the stability of physiological MREG_{BOLD} brain signal. Notably, CV can reflect joined effects of all physiological brain pulsations that cause signal variability (Kananen et al., 2018, 2020; Raitamaa et al., 2021; Tuovinen et al., 2020). The CV maps were calculated from pre-processed MREG_{BOLD} data (0.008–5 Hz) by normalizing the temporal standard deviation with mean signal intensity at each voxel (Figure 1). CV images were aligned with an isotropic 3 mm Montreal Neurological Institute (MNI) brain template and masked with an isotropic 3 mm MNI brain template to exclude any nonbrain voxels. While all calculations on CV maps were performed in 3 mm MNI space, CV images were aligned with an isotropic 1 mm MNI brain template for visualization purposes.

2.5 | Extracting tumor-related areas from FLAIR data

Since FLAIR imaging is regarded as one of the most sensitive neuroimaging methods for detecting white matter oedema in PCNSL, CV changes were compared against findings from T2-weighted FLAIR imaging. More specifically, mean CV values were examined from intratumoral areas, peritumoral areas, and the whole brain. The extent

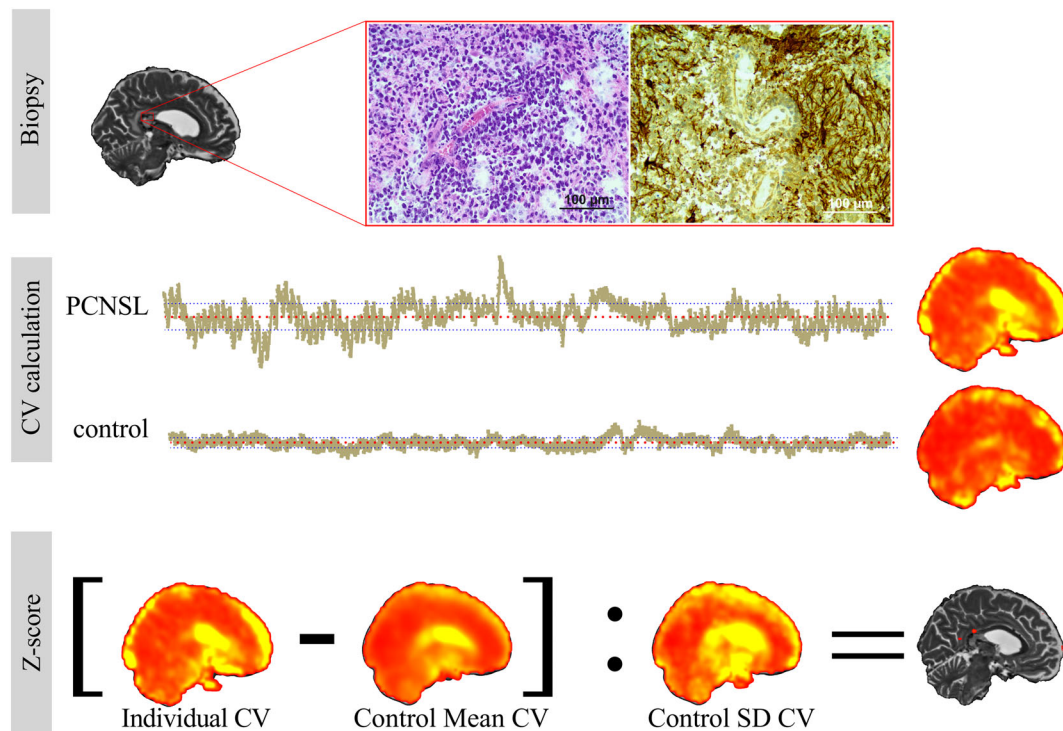


FIGURE 1 Coefficient of variation (CV) reflects stability of physiological brain signal and stability of physiological brain pulsations. Structural MRI data, fMRI data, and histological data is shown from a 65-year-old primary central nervous system lymphoma (PCNSL) patient and, for comparison, fMRI data from a healthy 56-year-old control subject. Upper panel: Using a stereotactic needle biopsy, histological analysis confirms PCNSL. The area of biopsy is highlighted on the T2-weighted image (red box). Histological staining of the acquired biopsy is shown with x20 magnification for haematoxylin-eosin staining (left) and glial fibrillary acidic protein (GFAP) staining (right). Both staining methods demonstrate a cerebral blood vessel whose perivascular space is obstructed by malignant lymphocytes. Additionally, GFAP staining shows that displaced astrocyte end-feet (dark brown) are unable to attach to the vascular endothelium. Middle panel: Pre-processed fMRI magnetic resonance encephalography (MREG_{BOLD}) signal (beige line; 0.008–5 Hz, 300 s) from a voxel within the biopsy area shown in the upper panel, and a corresponding signal from the healthy control subject. Respective CV maps are shown, whereby yellow indicates higher values. CV is calculated by normalizing the standard deviation (blue dotted line) with mean signal intensity (red dotted line). Therefore, CV reflects joined stability of physiological MREG_{BOLD} signal components and stability of physiological pulsations. Bottom panel: CV maps are transformed to Z-score maps by subtracting the control population's ($n = 30$) mean CV map from the individual PCNSL patient's CV map. The difference is normalized by the control population's ($n = 30$) standard deviation map. The resulting Z-CV map shows clusters, where the respective PCNSL patient's CV values exceed the control population mean by minimally three standard deviations ($Z \geq 3$). In this figure, the Z-CV map is superimposed on the patient's T2-weighted anatomical image.

of overlapping between CV changes and FLAIR changes was examined.

FLAIR images were first brain-extracted and aligned with an isotropic 1 mm Montreal Neurological Institute (MNI) brain template. FLAIR images were segmented manually by the first author using *fsleyes* tools, and a random sample was assessed by the last author who is an experienced neuroradiologist.

To acquire peritumoral areas for the calculation of mean CV values, segmented FLAIR images were first medium scale dilated with *fsmaths* tools. The segmented FLAIR images were then subtracted from the dilated images to create ring-like peritumoral areas. However, due to periventricular PCNSL location in some cases, some dilated FLAIR images contained voxels within CSF spaces whereas some contained only parenchymal voxels. Therefore, as a last step, a CSF mask was subtracted from all peritumoral masks to remove the effects of CSF pulsation and to concentrate analysis only to

parenchymal areas. To allow calculations between CV maps and segmented FLAIR maps, segmented FLAIR-maps were aligned with an isotropic 3 mm MNI brain template.

Mean CV values were calculated from multiple brain areas: whole brain, intratumoral areas, and peritumoral areas. The intratumoral and peritumoral areas were extracted using the hyperintense areas that are seen in FLAIR-imaging. Mean CV values were calculated from voxels that had nonzero values.

2.6 | Collecting prognostic models that use clinical performance scores or contrast-enhanced MRI

Since previously clinical performance scores such as the Memorial Sloan-Kettering Cancer Center (MSKCC) score have been linked to overall survival in PCNSL, MSKCC scores were compared against

respective whole brain mean CV values. The MSKCC score is an aggregation of age and pre-treatment Karnofsky performance status (KPS) score whereby higher class has been linked to worse outcome: MSKCC class 1 (age < 50y), MSKCC class 2 (age \geq 50y and KPS \geq 70), MSKCC class 3 (age \geq 50y and KPS < 70) (Abrey et al., 2006). MSKCC scores were collected before treatment and provided by an experienced neuro-oncologist.

Since findings from contrast-enhanced MRI have been linked to overall survival in PCNSL, whole brain mean CV values were compared against respective findings from T1-weighted contrast-enhanced imaging during the first diagnostic scan. Indeed, previously the International Extranodal Lymphoma Study Group (IELSG) model suggested that involvement of deep brain structures (periventricular regions, basal ganglia, brainstem, cerebellum) is an adverse factor in PCNSL (Ferreri et al., 2003). Other factors from contrast-enhanced MRI have been linked to prolonged overall survival, such as >1 brain lesions, involvement of multiple brain areas, and maximum tumor diameter (MTD) < 50 mm (Niparuck et al., 2019). Indeed, contrast-enhanced MRI data was collected from the first diagnostic MRI scan before dexamethasone and chemotherapeutic treatments. The contrast-enhanced data was assessed by the first author under the guidance of the last author who assessed unclear cases as an experienced neuroradiologist.

2.7 | Subject-level CV changes

Subject-level CV changes were detected by transforming CV values into Z-scores at each voxel (Kananen et al., 2018, 2020). The Z-score maps were calculated from each PCNSL patient using normative mean and standard deviation CV templates that were obtained from healthy controls (Figure 1). Threshold was applied at $Z \geq 3$ to highlight only those brain areas where CV values are substantially elevated.

2.8 | Distributions of subject-level CV changes and structural FLAIR changes

Since FLAIR lesions are regarded as the most sensitive and spatially the largest neuroimaging finding in PCNSL, spatial distributions of FLAIR lesions were compared against those of subject-level CV abnormalities ($Z \geq 3$). More specifically, spatial distributions of detected subject-level abnormalities were examined using topographical prevalence maps. To this end, Z-CV ($Z \geq 3$) or segmented FLAIR images were aggregated into respective group maps from which respective cumulative sums were calculated. To analyse the extent of overlap between patient-specific abnormalities, segmented FLAIR lesions and Z-CV maps ($Z \geq 3$) were multiplied together.

2.9 | Repeatable detection of CV changes

Follow-up data was available from 16 PCNSL patients. We aimed to test, whether clusters of abnormal CV values could be detected within

same areas in follow-up imaging using the same scanner. For this purpose, topographical incidence maps were formed: Z-CV maps ($Z \geq 3$) from follow-up MREG_{BOLD} scanning were aggregated into subject-specific templates and cumulative sums were calculated.

Moreover, to assess the stability of MREG_{BOLD} CV with other MRI scanners, we recruited an external population of healthy volunteer subjects ($n = 16$) that were for MREG_{BOLD} data in two different conditions—with the Vida scanner and with the Skyra scanner. In six subjects, the paired measurements were collected on the same day.

2.10 | Statistical analysis

Results were considered statistically significant when $p \leq .05$, and the normality for each parameter was calculated using normality-lognormality testing in Prism. Median values for age, absolute head displacement, relative head displacement, framewise head displacement, and whole brain mean CV values were compared between groups using exact two-tailed Mann–Whitney tests. Since respiration rate and heart rate may contribute towards fMRI BOLD signal variability, differences in respective parameters were calculated between groups using exact two-tailed Mann–Whitney tests. Sex proportions were compared across groups with an exact two-tailed Fisher's test. The difference between subject-level CV change volumes ($Z \geq 3$) and FLAIR lesion volumes were calculated using a two-tailed Wilcoxon signed-rank test (matched pairs) and their correlation using a Spearman coefficient. The correlations between whole brain mean CV values and respective relative or absolute head displacement was calculated using Spearman coefficients (matched pairs).

Prognostic variables were compared against whole brain mean CV values with Spearman correlation coefficients. To compare how whole brain mean CV values, MSKCC scores, or maximum tumor diameter may differentiate deceased and surviving PCNSL patients, ROC analysis was conducted. To this end, mean CV values were used from multiple brain areas: whole brain, intratumoral areas, peritumoral areas. Discriminating cut-off CV values were set based on highest likelihood ratio. Survival analysis was done with Kaplan–Meier analysis, whereby survival time was calculated from the first MREG_{BOLD} scan to the date of death from any reason. Survival curves were compared with a two-tailed log-rank test.

Groups' CV values were compared voxel-by-voxel using fMRI analysis tool LIPSIA with a nonparametric threshold-free permutation test that was adjusted for covariates and false discovery rate (Lohmann et al., 2018). More specifically, age, dexamethasone, and absolute head displacement were used as covariates. The number of permutations was set to 30,000. Age and head motion were used as regressors since they have previously been found to affect the fMRI BOLD signal, and dexamethasone was used as a regressor since it is generally accepted that structural lesions in diagnostic MRI may diminish after dexamethasone administration in PCNSL (Molnár et al., 1999). On the other hand, it is unknown how physiological brain pulsations react to dexamethasone.

Using the nonparametric threshold-free permutation tests, the independent effects of the following covariates were analysed separately with 30,000 permutations: age, dexamethasone, absolute head displacement, relative head displacement, framewise head displacement, opioids, and antiepileptics.

To compare Vida and Skyra MRI scanners in detecting CV changes in an external population of healthy volunteer control subjects ($n = 16$), CV maps from the two conditions were compared using a paired nonparametric threshold-free permutation tests using 30,000 permutations. In this testing, no covariates were used.

3 | RESULTS

3.1 | Demographics

Twenty-one pathologically confirmed PCNSL patients and 30 healthy age-matched controls were included in final analysis. Diagnosis was confirmed with stereotactic needle biopsy in 14 patients, excision in three patients, and fine needle CSF aspiration in two patients. In two of 21 patients, the exact method for biopsy (i.e., stereotactic biopsy versus excision) was not confirmed (Table 1).

Healthy control subjects (median 63y, range 14y) were age-matched with PCNSL patients (median 67y, range 29y) ($p = .057$) but the proportion of females was higher amongst healthy control subjects (21/30, 73%) than amongst PCNSL patients (8/21, 38%) ($p = .020$). While there was no difference in relative head displacement ($p = .99$) or in framewise displacement ($p = .68$), absolute head displacement was higher amongst PCNSL patients (median 0.21 mm) than amongst controls (median 0.16 mm) ($p = .012$). Respiration rates between PCNSL patients (median 0.26 Hz) and controls (median 0.25 Hz) did not differ ($p = .19$). Similarly, heart rates between PCNSL patients (median 1.19 Hz) and controls (median 1.12 Hz) did not differ ($p = .83$).

Importantly, MREG_{BOLD} datasets were acquired at early treatment phase before the first or second BBBD treatment. Twelve newly diagnosed PCNSL patients were scanned for MREG_{BOLD} after stereotactic biopsy or fine needle CSF aspiration, whereby the median time from stereotactic biopsy or CSF aspiration to MREG_{BOLD} acquisition was 31 days. In two of these 12 patients, the exact date of fine needle CSF aspiration or stereotactic biopsy was not recovered. Importantly, the anatomical effects of neurosurgical biopsy were assessed, whereby anatomical distortion was minimal after stereotactic needle biopsy (Figure S1).

Epileptic seizures were suspected in 10/21 (48%) PCNSL patients, based on witness-attested seizures or based on unwitnessed seizures. Six patients presented seizures as initial symptoms whereby one patient had previously been diagnosed with epilepsy but had remained asymptomatic. Four patients presented iatrogenic seizures during intra-arterial methotrexate infusion that is included within the BBBD-augmented therapy, or after autologous stem cell transplantation.

In this PCNSL population, 5/21 (24%) patients deceased during the study period. Four deceased patients had relapsed PCNSL while one had recent diagnosis. Importantly, all deceased patients were scanned before treatment. While deceased (66 y) and surviving PCNSL patients (69 y) were age-matched ($p = .21$) and relative head displacement showed no differences ($p = .31$), absolute head displacement was higher amongst deceased patients (median 0.41 mm) than amongst surviving patients (median 0.19 mm) ($p = .040$). Framewise head displacement did not differ between deceased (median 0.090 mm) and surviving (median 0.062 mm) PCNSL patients ($p = .31$) (Table 1).

3.2 | Increased CV is linked to short-term mortality

All deceased patients revealed markedly higher whole brain mean CV values ($n = 5$, median 0.055) than surviving patients ($n = 16$, median 0.028) ($p < .0001$). Notably, one patient with an elevated whole brain mean CV value was still alive during analysis but deceased within weeks. Based on receiver operating characteristics (ROC) analysis, a cut-off whole brain CV value was set at 0.042 with 100% sensitivity and 100% specificity. Based on this cut-off value, Kaplan-Meier survival analysis demonstrated that survival probability was lower amongst patients with high whole brain mean CV values (median survival time 0.70 years, 1-year survival probability 20%) than amongst patients with lower whole brain mean CV values (all survived) ($p < .0001$) (Figure 2). Indeed, higher whole brain mean CV values were linked to high death probability (Hazard Ratio 109; 95% CI [13 to 927]). Interestingly, whole brain CV outperformed both intratumoral CV (AUC = 0.83, $p = .032$) and peritumoral CV (AUC = 0.78, $p = .069$) in differentiating deceased PCNSL patients from surviving PCNSL patients.

Whole brain mean CV values in PCNSL patients did not correlate with absolute motion (Spearman $r_s = .32$, $p = .16$) or with relative motion ($r_s = .28$, $p = .22$), respectively. Conversely, whole brain mean CV values in healthy controls correlated with both absolute motion ($r_s = .56$, $p = .0007$) and with relative motion ($r_s = .57$, $p = .001$), respectively (data not shown).

3.3 | Mean CV values are independent of prognostic performance scores and contrast-enhancement

Whole brain mean CV values were, respectively, compared against prognostic MSKCC performance scores, the number of contrast-enhancing foci, and the maximum tumor diameter (MTD) in contrast-enhanced MRI. Considering that the number of contrast-enhancing foci varied between 1 and 6, maximum MTD was calculated from the single largest lesion whereas total MTD was calculated as the sum of all MTD values (Table S2).

As FLAIR imaging is routinely used in clinical neuroimaging since it is considered sensitive for detecting white matter oedema, we first

TABLE 1 Demographics

Characteristic	PCNSL (n = 21)	Controls (n = 30)	p value
Females (n)	8 (38%)	22 (73%)	.020*
Age (years)	67 (29)	63 (14)	.057
Absolute head displacement (mm)	0.21 (1.0)	0.16 (0.40)	.012*
Relative head displacement (mm)	0.036 (0.041)	0.036 (0.040)	.99
Frame-wise displacement (mm)	0.063 (0.078)	0.062 (0.068)	.68
Respiratory rate (Hz)	0.26 (0.29)	0.25 (0.22)	.19
Heart rate (Hz)	1.19 (0.61)	1.12 (1.01)	.83
Method for diagnosis			
CSF aspiration	2 (9.5%)		
Stereotactic needle biopsy	14 (67%)		
Excision	3 (14%)		
Unconfirmed method of biopsy	2 (9.5%)		
Comorbidities			
Hypertension	8 (38%)	7 (23%)	
Hypercholesterolemia	5 (24%)	6 (20%)	
Arrhythmia	4 (19%)	0 (0%)	
Musculoskeletal	3 (14%)	0 (0%)	
Psychiatric	2 (10%)	0 (0%)	
Hypothyroidism	3 (14%)	2 (7%)	
Diabetes	2 (10%)	0 (0%)	
Asthma	0 (0%)	3 (10%)	
Glaucoma	1 (5%)	2 (7%)	
Unclassified	6 (29%)	3 (10%)	
Epileptic seizures (n)			
iatrogenic	4 (40%)	0 (0%)	
Initial symptoms	6 (60%)	0 (0%)	
Medication (n)			
Phenytoin	12 (57%)		
Dexamethasone	7 (33%)		
Tramadol	4 (19%)		
Treatment phase during MREG (n)			
Relapse			
Pre-treatment 1	6 (29%)		
New diagnosis			
Pre-treatment 1 (pre-intervention ^a)	3 (14%)		
Pre-treatment 1 (postintervention)	7 (33%)		
Pre-treatment 2	5 (24%)		
Time from diagnosis to MREG (d) ^b	31 (52)		
Re-scan interval (weeks)	5 (14)		
Deceased patients (n)			
Females (n)	1 (20%)		
Age (years)	66 (15)		
Absolute head displacement (mm)	0.41 (0.33)		
Relative head displacement (mm)	0.050 (0.038)		
Frame-wise displacement (mm)	0.090 (0.070)		
Relapses, pre-treatment 1 (n)	4 (80%)		

TABLE 1 (Continued)

Characteristic	PCNSL (n = 21)	Controls (n = 30)	p value
New diagnosis, pre-treatment 1 (n)	1 (20%)		
Survival time after MREG (months)	9.2 (17.2)		
Surviving patients (n)	16 (76%)		
Age (years)	69 (29)		
Absolute head displacement (mm)	0.19 (1.0)		
Relative head displacement (mm)	0.035 (0.031)		
Framewise displacement (mm)	0.062 (0.059)		

Note: Values represent median and corresponding range, or number and corresponding frequency. For differences in sex distributions, the *p* value represents an exact two-tailed Fisher's test. For other characteristics, *p* values represent exact two-tailed Mann-Whitney tests. *Significant *p* values. Abbreviation: PCNSL, primary central nervous system lymphoma.

^aIntervention is defined as stereotactic needle biopsy, excision, or fine needle cerebrospinal fluid (CSF) aspiration.

^bWhile 12 newly diagnosed PCNSL patients were scanned for MREG_{BOLD} data after CSF aspiration or stereotactic biopsy, the exact date was recovered in 10 PCNSL patients.

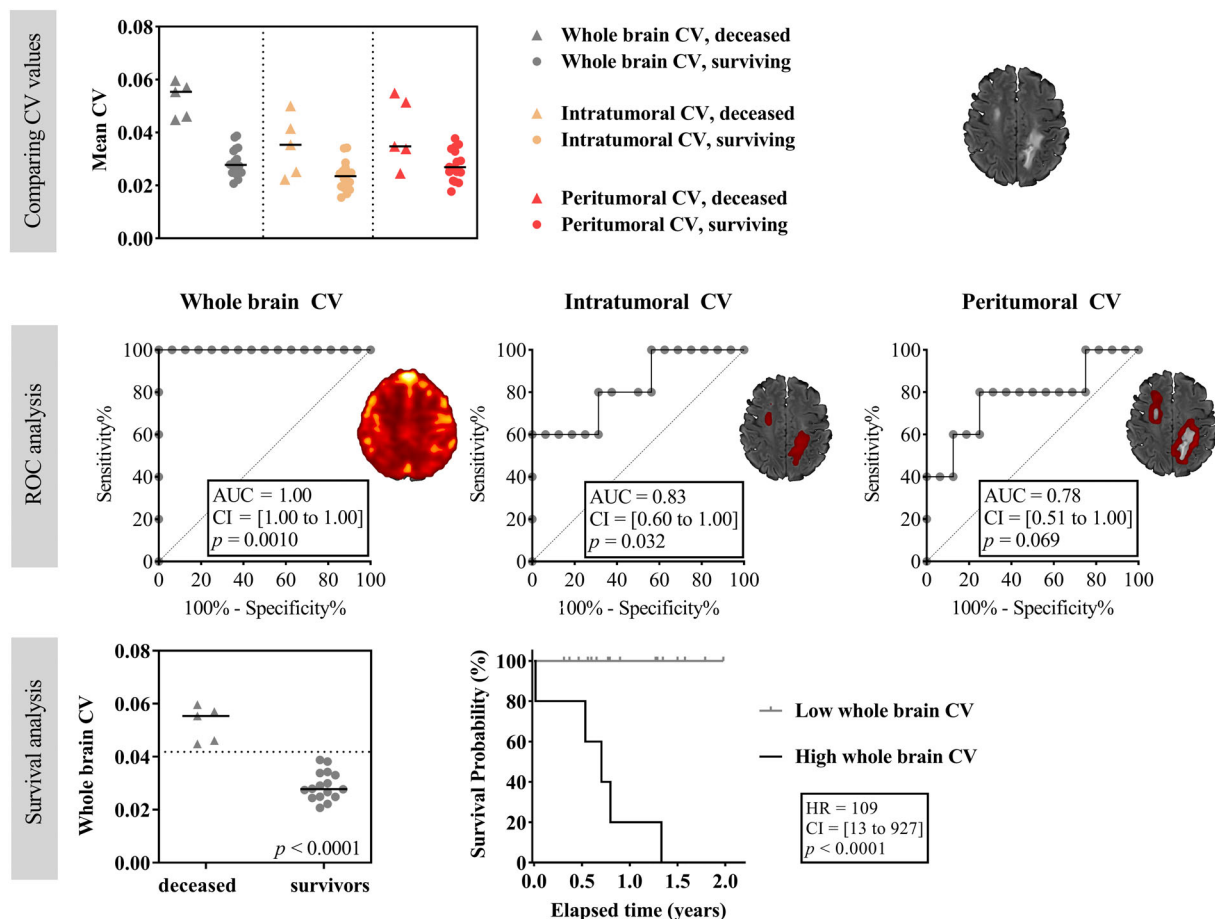


FIGURE 2 Increased mean coefficient of variation (CV) values are linked to short-term mortality in primary central nervous system lymphoma (PCNSL). Top panel: Mean CV values are compared between deceased PCNSL patients (*n* = 5) and surviving PCNSL patients (*n* = 16) using various regions of interest (whole brain, intratumoral areas, and peritumoral areas). Intratumoral and peritumoral regions are determined from T2-fluid attenuated inversion recovery (FLAIR) images. Short horizontal black lines represent group median. Middle panel: Receiver operating characteristic (ROC) analysis using the mean CV values that are seen in the upper panel. The respective brain images demonstrate, using one PCNSL patient, the regions of interest that are used for mean CV value calculation. The CV maps are superimposed on to the patient's FLAIR image. Bottom panel: Survival analysis using whole brain mean CV values. Left graph is a magnification of the top panel graph, whereby the dotted horizontal line represents a cut-off value for differentiating deceased and surviving PCNSL patients with 100% sensitivity and 100% specificity. The *p* value represents results from an exact two-tailed Mann-Whitney test. Right graph shows respective Kaplan-Meier survival curves for patients with high CV values and for patients with low CV values with relation to the dotted cut-off value that is seen in the left graph. The *p* value represents results from a two-tailed log-rank test. AUC, area under curve; CI, 95% confidence interval of AUC values

compared prognostic parameters against respective FLAIR volumes. FLAIR volume during MREG_{BOLD} acquisition correlated with whole brain mean CV values ($r_s = .48, p = .028$) and surprisingly with maximum MTD ($r_s = .46, p = .038$), but not with total MTD ($r_s = .27, p = .23$) nor with multifocality ($r_s = -.21, p = .37$) from pre-treatment contrast-enhanced MRI. Additionally, FLAIR volumes did not correlate with MSKCC scores ($r_s = .048, p = .84$) (data not shown).

While whole brain mean CV values correlated with FLAIR volumes as shown above, whole brain mean CV values did not correlate with maximum MTD ($r_s = .24, p = .29$), total MTD ($r_s = .34, p = .13$), or with multifocality ($r_s = .071, p = .76$). Similarly, whole brain mean CV values did not correlate with MSKCC scores ($r_s = .27, p = .24$) (Figure S2).

Additionally, we aimed to examine if deceased PCNSL patients could be discriminated from surviving PCNSL patients using prognostic factors. To this end, we compared MSKCC scores (AUC = 0.66, $p = .30$), maximum MTD (AUC = 0.54, $p = .80$), total MTD (AUC = 0.56, $p = .68$), and multifocality (AUC = 0.52, $p = .90$) that did not confidently discriminate surviving PCNSL patients from deceased PCNSL patients. Contrarily, FLAIR volumes during MREG_{BOLD} acquisition were able to discriminate deceased and surviving PCNSL patients (AUC = 0.82, $p = .039$) (data not shown).

3.4 | Increased CV differentiates PCNSL patients from healthy controls

PCNSL patients revealed higher whole brain mean CV values (median 0.030) than healthy age-matched controls (median 0.023) ($p = .0002$). Furthermore, ROC-analysis demonstrated that whole brain mean CV values differentiate patients from controls (AUC = 0.80). The cut-off value was set according to highest likelihood ratio (12.9) at CV = 0.034 with 43% sensitivity and 97% specificity (Figure 3).

3.5 | Group-level CV changes are found within all over the brain

To test voxel-by-voxel differences in CV, we conducted nonparametric threshold-free permutation tests that were adjusted for covariates (age, dexamethasone, absolute head displacement) and for false discovery rate. PCNSL brains revealed greater CV values (group median 0.035) than healthy age-matched control brains (group median 0.024). The voxel-by-voxel nonparametric test showed significantly increased CV ($p \leq .001$, corrected for false discovery rate) in some areas where PCNSL is most frequently detected with diagnostic MRI (Cheng & Zhang, 2019; Haldorsen et al., 2009; Küker et al., 2005; Mansour et al., 2014). More precisely, significantly increased CV was detected within cerebral white matter, corpus callosum, cerebral cortices (subcallosal cortex, insular cortex), cerebellum, brainstem, cortical gyri, and ventricles of PCNSL brain. Interestingly, significant CV differences localized around posterior, median, and anterior cerebral artery territories (Figure 4). After excluding deceased patients ($n = 5$) from

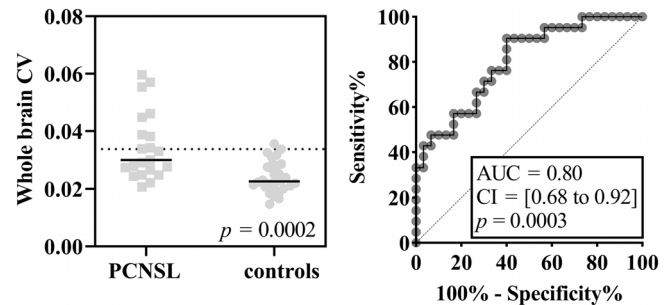


FIGURE 3 Whole brain mean coefficient of variation (CV) values differentiate primary central nervous system lymphoma (PCNSL) patients from healthy controls. Left graph: Whole brain mean CV values from all PCNSL patients ($n = 21$) and from healthy age-matched controls ($n = 30$). The p value represents results from an exact two-tailed Mann-Whitney test. Short horizontal black lines represent group median, and dotted horizontal line represent cut-off value for differentiating these groups with 43% sensitivity and 97% specificity. Right graph: Receiver operating characteristic (ROC) analysis using those whole brain mean CV values that are shown in the left graph. AUC, area under curve; CI, 95% confidence interval of AUC values.

analysis due to quality assurance, CV differences persisted within the same areas (data not shown).

Independent effects of the following covariates were analysed separately: age, dexamethasone, absolute head displacement, relative head displacement, framewise displacement, opioids, and antiepileptics. Only framewise displacement affected the difference in CV. Significant effects were seen within frontal areas of the sagittal sinus and these areas did not overlap with the areas where significant differences in CV were seen. Indeed, these these sinus areas may present respiration-related motion artefacts (Figure S3).

3.6 | Subject-level CV changes are found within CSF areas and parenchyma

Increased CV values were found at subject-level using Z-CV maps ($Z \geq 3$), wherein highlighted clusters showed only markedly increased CV values. Depending on the subject, respectively, markedly increased CV values were found within cerebral white matter, cerebral cortices, cortical gyri, and ventricles. The CV changes extended beyond tissue FLAIR hyperintensities and contrast-enhancing lesions in all PCNSL patients (Figure 5). Interestingly, a Z-CV map taken before any treatment from one PCNSL patient demonstrated a periventricular cluster near an area that later revealed PCNSL relapse (Figure 6).

3.7 | Subject-level CV changes extend spatially further than aberrant findings in diagnostic MRI

Topographical prevalence maps were used to investigate spatial distributions of imaging abnormalities. FLAIR lesions distributed within

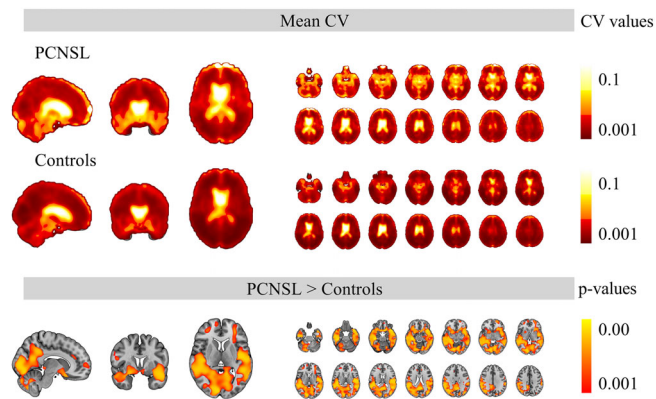


FIGURE 4 Increased coefficient of variation (CV) in primary central nervous system lymphoma (PCNSL). CV from physiological magnetic resonance encephalography (MREG_{BOLD}) sequence data (0.008–5 Hz) reflects stability of all physiological signal sources and stability of all physiological pulsations. Upper panel: Mean CV value maps from PCNSL patients ($n = 21$) and from healthy age-matched controls ($n = 30$). Lower panel: A nonparametric threshold-free permutation test that has been adjusted for covariates (age, dexamethasone, absolute head displacement). Significant CV differences localize around arterial territories ($p \leq .001$, corrected for false discovery rate, 30,000 permutations). Anatomical background image is a standard T1-weighted Montreal neurological institute template, coordinates [10, 5, 7].

periventricular white matter whilst abnormally pulsating clusters ($Z \geq 3$) distributed to a greater extent within cerebral cortices and deeper within cerebral white matter. The volumes for Z-CV clusters (median $1.10 \times 10^5 \text{ mm}^3$) and FLAIR lesion (median $0.62 \times 10^5 \text{ mm}^3$) correlated (Spearman $r_s = .51$, $p = .018$) but differed ($p = .0055$). Interestingly, most clusters with elevated CV values were found outside tissue FLAIR hyperintensities (median 98% of volume) (Figure 7).

3.8 | CV mapping is repeatable

We aimed to assess the repeatability of CV mapping using the same MRI scanner. Follow-up data was available for 16/21 (76%) PCNSL patients, and the median follow-up interval was 5 weeks (range 14 weeks). One patient yielded five MREG_{BOLD} scans and some CV changes were detected in *all five* scans, which highlights the repeatability of this signal stability metric. Repeatable CV changes were found in occipital, temporal and frontobasal areas that included white matter, grey matter, and tumour of this patient. Notably, most of these clusters with aberrant CV values were not detected in FLAIR imaging. Additional two patients yielded four MREG_{BOLD} scans each, and both revealed similar repeatedly detected clusters (Figure S4).

We also aimed to test the stability and repeatability of CV mapping with different MRI scanners. To this end, CV maps from the two conditions (Vida scanner and Skyra scanner) were compared with paired nonparametric threshold-free permutation tests. Critically, CV values from Vida and Skyra were comparable within brain

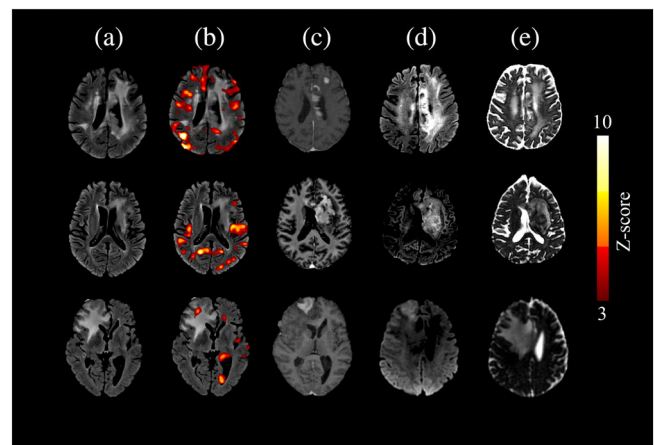


FIGURE 5 Subject-level findings of increased coefficient of variation (CV) in primary central nervous system lymphoma (PCNSL). Top row: 69-year-old female with dizziness and headache. The patient was deceased after 6 months of initial symptoms (pre-biopsy scan). Middle row: 70-year-old male with symptoms of depression and disorientation (postbiopsy scan, pre-treatment). Bottom row: 71-year-old female with gradual memory loss, fatigue, and disorientation (pre-biopsy scan). (a) T2-weighted fluid-attenuated inversion recovery (FLAIR) data (b) physiological magnetic resonance encephalography (MREG_{BOLD}) sequence data. Clusters show, where CV values are increased as a sign of increased physiological brain signal instability and physiological pulsation instability. The threshold $Z \geq 3$ includes only CV values that exceed the control population mean by three standard deviations. (c) Contrast-enhanced T1-weighted data. (d) Diffusion-weighted image (DWI). (e) Apparent diffusion coefficient (ADC) data. Note that intensity changes may be seen on different slice levels depending on the sequence.

parenchyma. However, differences in CV were found within ventricular CSF areas ($p \leq .05$, corrected for false discovery rate) (Figure S5).

4 | DISCUSSION

Previous studies suggest primary central nervous system lymphoma (PCNSL) invasion cannot be fully detected with current diagnostic imaging, and there are no simple prognostic tools that can be utilized when selecting patients for advanced therapy. Since previous physiological imaging studies have found abnormal cerebrovascular pulsation in diseases affecting the (peri)vascular space, we hypothesized that the documented (peri)vascular PCNSL involvement alters cerebrovascular pulsation even in radiologically intact brain areas. We calculated the Coefficient of Variation (CV) from physiological magnetic resonance encephalography (MREG_{BOLD}) signal to quantify the instability of physiological brain pulsations. Increased CV was linked to short-term mortality in pre-treatment scanning and in line with the perivascular whole brain infiltration pattern of PCNSL, group-level CV differences were found across the brain and mostly localizing around arterial territories. Notably, subject-level CV changes extended spatially beyond tissue fluid-attenuated inversion recovery (FLAIR) hyperintensities, suggesting that PCNSL causes physiological instability in

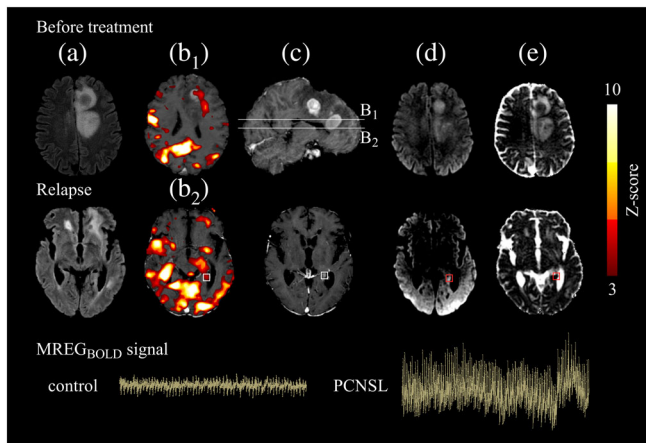


FIGURE 6 Increased coefficient of variation (CV) near an area that later developed radiologically confirmed primary central nervous system lymphoma (PCNSL) relapse in one patient. Data is shown from a PCNSL patient, who was scanned before any treatment and after 6 months at relapse. White and red boxes show the area of contrast-enhancing relapse. The patient deceased within months. (a) T2-weighted fluid-attenuated inversion recover (FLAIR) data. (b) Physiological magnetic resonance encephalography (MREG_{BOLD}) data superimposed on respective row's T1-weighted contrast-enhanced images. Clusters show, where CV is markedly increased as a sign of increased physiological brain signal instability ($Z \geq 3$) and physiological instability. Note that both B₁ and B₂ demonstrate different slice levels of the same MREG_{BOLD} data that was obtained before treatment; slice levels are noted in image C. (c) Contrast-enhanced T1-weighted data. (d) Diffusion-weighted image (DWI). (e) Apparent diffusion coefficient (ADC) data. Note that intensity changes may be seen on different slice levels depending on the sequence. Bottom row: MREG_{BOLD} signal from the cluster noted in B₂ (white box). For comparison, a healthy control subject's MREG_{BOLD} signal is shown from the same area.

radiologically intact brain regions. Interestingly, one patient revealed CV changes near an area that developed PCNSL relapse after 6 months. CV values were independent of clinical performance scores and findings from contrast-enhanced MRI.

4.1 | Sources of CV changes

T2*-weighted fMRI brain BOLD signal has been commonly used to map slow (<0.1 Hz) changes in regional blood flow and oxygenation that follow neural activation (Fox & Raichle, 2007; Ogawa et al., 1992). On that note, some components of the blood-brain barrier, such as pericytes and astrocytes, modulate regional blood flow and therefore may contribute to the BOLD signal in health and in disease (Hall et al., 2014). However, since the T2*-weighted BOLD signal is a summation of multiple physiological sources of signal variability, it also encompasses respiratory and cardiovascular brain pulsations that arise from CSF pulsation and from cardiac-induced vascular pulsation that can be detected with critically sampled BOLD fMRI (Dreha-Kulaczewski et al., 2017; Glover et al., 2000; Kiviniemi et al., 2016;

Posse et al., 2013; Raitamaa et al., 2021; Rajna et al., 2021; Tuovinen et al., 2020). Notably, the physiological pulsations traverse through the whole brain reflecting brain pulsation in grey matter, white matter, and in CSF spaces.

MREG_{BOLD} signal CV indicates signal stability, or the extent to which the physiological signal varies as a proportion to its baseline intensity. Since CV can reflect all signal variation sources, BOLD signal variability is altered in multiple instances including Alzheimer's disease (Makedonov et al., 2016; Tuovinen et al., 2020), aging or small vessel disease (Makedonov et al., 2013), acute ischaemic stroke (Khalil et al., 2017), chronic kidney disease (Jahani et al., 2014), CO₂ fluctuations (Wise et al., 2004), epilepsy (Kananen et al., 2018, 2020) and arterial stiffness (Hussein et al., 2020). Previous studies have also linked altered fMRI brain signal variability to reduced arterial wall elasticity and declining glymphatic fluid clearance in some neurological diseases (Rajna et al., 2021; Tuovinen et al., 2020). Notably, previous studies have found physiological MREG_{BOLD} signal changes even in otherwise radiologically intact brain areas (Kananen et al., 2018, 2020; Rajna et al., 2021; Tuovinen et al., 2020). Taken together, BOLD signal CV has been linked to physiological instability and (peri)vascular properties such as (neuro)vascular degeneration, cerebrovascular reactivity, CSF flow, and cerebral blood volume (Jahani et al., 2014; Kananen et al., 2018, 2020; Makedonov et al., 2013, 2016), and therefore fMRI may provide methods for studying (peri)vascular function in PCNSL.

4.2 | PCNSL and CV changes

Ultrastructural evidence shows that PCNSL invasion occludes the perivascular space, causes loss of small capillaries, and markedly alters (peri)vascular components with respect to variable endothelium thickness, variable basal lamina thickness, endothelial discontinuation, and astrocyte reactions (Aho et al., 1993; Molnár et al., 1999; O'Connor et al., 2019). Since neovascularisation is relatively minimal in PCNSL, perfusion imaging indicates hypoperfusion and for blood supply, PCNSL recruits pre-existing host vasculature (Donnem et al., 2013; Liu et al., 2019; Xing et al., 2014). Interestingly, the malignant lymphoma cells and their perivascular environment also express vasoactive substances that have been linked to immune escaping (Sugita et al., 2015).

While the marked histological effects of perivascular PCNSL invasion have been well documented using neurosurgical biopsies from radiologically aberrant brain regions, the histology of radiologically intact brain regions has not been extensively studied. However, previous studies suggest that lymphocytes may invade along enlarged perivascular spaces without disrupting the BBB and thus invasion in radiologically intact brain regions may be possible (Aho et al., 1993; Ambady et al., 2017). Previous studies have also suggested that PCNSL seeding could be transmitted from radiologically occult lymphoma reservoirs via CSF flow (Ambady et al., 2017).

We detected subject-level CV changes in CSF spaces. Considering that previous fMRI studies have found strong physiological

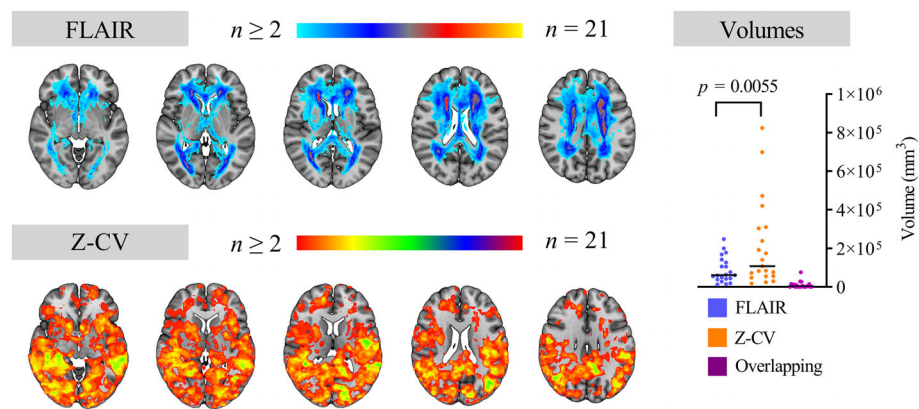


FIGURE 7 Topography of abnormal imaging findings in primary central nervous system lymphoma (PCNSL). Upper left panel: Topographical prevalence map of fluid-attenuated inversion recovery (FLAIR) abnormalities. Lower left panel: Topographical prevalence map of abnormal coefficient of variation (CV) values where CV values are markedly increased ($Z \geq 3$) as a sign of physiological instability. Colour-encoded values represent the number of subjects (n) with abnormal imaging findings in a population of 21 PCNSL patients. Right panel: Volumes of detected abnormalities. Additionally, the extent of spatial overlap between respective findings is shown for each patient. Horizontal black lines represent median volumes, and the p value illustrates results from a two-tailed Wilcoxon signed-rank test (matched pairs). Anatomical background image is a standard T1-weighted Montreal neurological institute template.

pulsation distinctly within CSF spaces and (peri)arterial areas (Dreha-Kulaczewski et al., 2017; Glover et al., 2000; Raitamaa et al., 2021), our findings of anatomically localized subject-level CV changes within CSF spaces may be linked to aberrant CSF pulsation. Furthermore, since we found statistically significant group-level CV differences around arterial territories, we hypothesize that the physiological instability is likely linked to (peri)vascular alterations. Indeed, considering the possibility of perivascular obstruction in radiologically preserved brain regions (Aho et al., 1993; Ambady et al., 2017), physiological instability in PCNSL may be linked to aberrant CSF flow. Furthermore, since fMRI BOLD signal may be modulated by astrocyte function (Hall et al., 2014), the documented astrocyte reactions and structural BBB alterations in PCNSL may also be linked to physiological instability (Aho et al., 1993; O'Connor et al., 2019). Finally, considering that BOLD signal CV has previously been linked to cerebral blood volume, the documented loss of capillaries in PCNSL may additionally be linked to the instability of physiological MREG_{BOLD} signal.

4.3 | Strengths, limitations, and prospects

Since *absolute* head displacement differed between deceased and surviving patients and between PCNSL patients and healthy controls, data de-spiking was used in pre-processing to minimize confounding effects. Notably, nonparametric voxel-by-voxel analysis within LIPSIA demonstrated that age, medication, head motion, and cardiorespiratory rates that could affect the stability of fMRI BOLD signal did not demonstrate any effect on CV differences. Regardless, to minimize confounding effects, the nonparametric permutation tests within LIPSIA were adjusted for age, dexamethasone, and absolute head displacement. Framewise displacement affected the differences in CV within areas that did not overlap with areas that presented significant

differences in CV. Patients and controls had comorbidities that could have confounding effects (Table 1).

Due to fast sampling of MREG_{BOLD} and the large number of acquired datapoints, we were able to perform subject-level analysis. Notably, while Z-values should not be interpreted directly as p values, Z-score maps demonstrated markedly increased CV values that were repeatedly detected in up to five scans of the same patient. Additionally, using an external population of 16 healthy control subjects, we assessed the stability and repeatability for CV mapping using different MRI scanners. Critically, Vida and Skyra scanners yielded comparable MREG_{BOLD} CV values within brain parenchyma. However, differences in CV were seen within ventricular CSF areas.

Whilst our results indicate that PCNSL increases MREG_{BOLD} signal CV, the exact source of physiological brain signal instability remains unknown and therefore spectral signal properties need to be further addressed. Physiological signal changes must also be correlated with histopathological findings. In this short-term study, the number of deceased patients was relatively small (5/21, 24%) since BBB chemotherapy followed by high-dose treatment and autologous stem cell transplantation yields curative results in 80% of patients (Angelov et al., 2009; Kuitunen et al., 2017), and therefore we do not have access to extensive histological analysis.

Twelve newly diagnosed PCNSL patients were scanned for MREG_{BOLD} after stereotactic biopsy or fine needle aspiration whereby the median time from intervention was 31 days, which is likely to reduce acute tissue responses during MREG_{BOLD} acquisition. Stereotactic needle biopsy is considered mini-invasive, and in this study the anatomical distortion after stereotactic biopsy was minimal. Regardless, postoperative changes may include leakage of blood products with magnetic properties, and oedema. While we did not have access to susceptibility-weighted imaging in this PCNSL population, we conclude that anatomical distortion was confined to spatially restricted

areas and do not affect whole brain CV. However, we did not have access to susceptibility-weighted imaging in this PCNSL population. Notably, the MREG sequence exhibits better off-resonance behavior and suffers less from susceptibility-related artefacts than EPI-based fMRI sequences due to spiral k-space acquisition (Hennig et al., 2021).

The retrospective nature of this study is a limitation. Indeed, while we found a link between whole brain mean CV values and mortality in all five deceased PCNSL patients, possible prognostic value of CV mapping needs to be further studied. More precisely, future studies need to prospectively stratify PCNSL patients into subgroups based on whole brain mean CV values and finally compare mortality between subgroups. Larger study sizes will also be needed when constructing a potential prognostic model in this rare disease. While analysis in this study was conducted retrospectively, MREG_{BOLD} data was obtained from deceased patients before treatment. Notably, one deceased PCNSL patient showed an elevated whole brain mean CV value while still alive.

In this study we found that CV was independent of prognostic MSKCC performance scores and independent of findings in T1-weighted contrast-enhanced imaging but correlated with findings from FLAIR imaging. However, FLAIR data and contrast-enhanced data were not assessed by an experienced neuroradiologist and therefore a margin of error is possible. Additional prognostic models containing CSF analysis, serum analysis, and histological staining will have to be assessed in the future (Ferreri et al., 2003).

In the future, chemotherapy may be noninvasively augmented by transiently opening the intact BBB with focused ultrasound (Meng et al., 2019). Notably, we repeatedly found clusters of elevated CV values in up to five follow-up scans of the same patient, and we also found a cluster of abnormal CV values near an area that later evolved PCNSL relapse. While repeatedly detected clusters could provide therapeutic foci in PCNSL, the relapse patterns, histological correlations, and physiological fMRI signal changes need to be further addressed simultaneously.

5 | CONCLUSION

This is the first study in PCNSL that analyses physiological brain pulsations. Our results suggest that perivascular PCNSL infiltration causes instability of physiological pulsations in otherwise radiologically intact vascular territories. Furthermore, this data suggests that noninvasive CV may be linked to short-term mortality in PCNSL despite a promising treatment regimen.

AUTHOR CONTRIBUTION

Conception of study: Valter Poltojaime, Timo Tuovinen, Matti Järvelä, Janne Kananen, Vesa Kiviniemi. Data Acquisition: Valter Poltojaime, Janette Kempainen, Nina K. Keinänen, Juha-Matti Isokangas, Hanne Kuitunen, Juha Nikkinen, Eila Sonkajärvi, Vesa Korhonen, Tommi K. Korhonen, Sami T. Tetri, Outi Kuittinen, Vesa Kiviniemi. Analysis: Valter Poltojaime, Vesa Korhonen, Niko Huotari, Lauri J. Raitamaa. Interpretation: Valter Poltojaime,

Michaela K. Bode, Vesa Kiviniemi. All authors have contributed to this draft. All authors have approved the final version of this manuscript. All authors have agreed to be accountable for all aspects of this work in ensuring that questions related to the accuracy or integrity of this work are appropriately investigated and resolved.

ACKNOWLEDGEMENTS

The authors wish to acknowledge CSC (IT Centre for Science, Finland) for its computational resources. The authors also wish to thank Annastiina Kivipää and Matti Pasanen for data acquisition, and Jussi Kantola for computational assistance.

CONFLICT OF INTEREST

The authors declare no conflict of interest.

DATA AVAILABILITY STATEMENT

The data that support the findings of this study are available from the corresponding author upon reasonable request.

ETHICS STATEMENT

This study adheres to the Declaration of Helsinki and institutional approval was granted by the Ethical Committee of Northern Ostrobothnia Hospital District, Oulu University Hospital. Written informed consent was obtained from all subjects.

ORCID

Valter Poltojaime  <https://orcid.org/0000-0003-1105-1076>

Lauri Raitamaa  <https://orcid.org/0000-0003-2884-6510>

Janne Kananen  <https://orcid.org/0000-0001-6831-8056>

Vesa Kiviniemi  <https://orcid.org/0000-0003-0184-8524>

REFERENCES

- Abrey, L. E., Ben-Porat, L., Panageas, K. S., Yahalom, J., Berkey, B., Curran, W., Schultz, C., Leibel, S., Nelson, D., Minesh, M., & DeAngelis, L. M. (2006). Primary central nervous system lymphoma: The Memorial Sloan-Kettering Cancer Center prognostic model. *Journal of Clinical Oncology*, 24(36), 5711–5715.
- Aho, R., Ekfors, T., Haltia, M., & Kalimo, H. (1993). Pathogenesis of primary central nervous system lymphoma: Invasion of malignant lymphoid cells into and within the brain parenchyma. *Acta Neuropathologica*, 86(1), 71–76.
- Ambady, P., Rongwei, F., Netto, J. P., Kersch, C., Firkins, J., Doolittle, N. D., & Neuwelt, E. A. (2017). Patterns of relapse in primary central nervous system lymphoma: Inferences regarding the role of the neuro-vascular unit and monoclonal antibodies in treating occult CNS disease. *Fluids Barriers CNS*, 14(1), 16.
- Angelov, L., Doolittle, N. D., Kraemer, D. F., Siegal, T., Barnett, G. H., Peereboom, D. M., Stevens, G., McGregor, J., Jahnke, K., Lacy, C. A., Hedrick, N. A., Shalom, E., Ference, S., Bell, S., Sorenson, L., Tyson, R. M., Haluska, M., & Neuwelt, E. A. (2009). Blood-brain barrier disruption and intra-arterial methotrexate-based therapy for newly diagnosed primary CNS lymphoma: A multi-institutional experience. *Journal of Clinical Oncology*, 27(21), 3503–3509.
- Assländer, J., Zahneisen, B., Hugger, T., Reisert, M., Lee, H. L., LeVan, P., & Hennig, J. (2013). Single shot whole brain imaging using spherical stack of spirals trajectories. *NeuroImage*, 73, 59–70.

- Cheng, G., & Zhang, J. (2019). Imaging features (CT, MRI, MRS, and PET/CT) of primary central nervous system lymphoma in immunocompetent patients. *Neurological Sciences*, 40(3), 535–542.
- Donnem, T., Hu, J., Ferguson, M., Adighibe, O., Snell, C., Harris, A. L., Gatter, K. C., & Pezzella, F. (2013). Vessel co-option in primary human tumors and metastases: An obstacle to effective anti-angiogenic treatment? *Cancer Medicine*, 2(4), 427–436.
- Dreha-Kulaczewski, S., Joseph, A. A., Merboldt, K. D., Ludwig, H. C., Gärtner, J., & Frahm, J. (2017). Identification of the upward movement of human CSF in vivo and its relation to the brain venous system. *The Journal of Neuroscience*, 37(9), 2395–2402.
- Ferreri, A. J. M., Blay, J. Y., Reni, M., Pasini, F., Spina, M., Ambrosetti, A., Calderoni, A., Rossi, A., Vavassori, V., Conconi, A., Devizzi, L., Berger, F., Ponzoni, M., Borisch, B., Tinguely, M., Cerati, M., Milani, M., Orvieto, E., Sanchez, J., ... Cavalli, F. (2003). Prognostic scoring system for primary CNS lymphomas: The international Extranodal lymphoma study group experience. *Journal of Clinical Oncology*, 21(2), 266–272.
- Fox, M. D., & Raichle, M. E. (2007). Spontaneous fluctuations in brain activity observed with functional magnetic resonance imaging. *Nature Reviews Neuroscience*, 8(9), 700–711.
- Glover, G. H., Li, T. Q., & Ress, D. (2000). Image-based method for retrospective correction of physiological motion effects in fMRI: RETRO-ICOR. *Magnetic Resonance in Medicine*, 44(1), 162–167.
- Grommes, C., & DeAngelis, L. M. (2017). Primary CNS lymphoma. *Journal of Clinical Oncology*, 35(21), 2410–2418.
- Haldorsen, I. S., Kråkenes, J., Krossnes, B. K., Mella, O., & Espeland, A. (2009). CT and MR imaging features of primary central nervous system lymphoma in Norway, 1989–2003. *American Journal of Neuroradiology*, 30(4), 744–751.
- Hall, C. N., Reynell, C., Gesslein, B., Hamilton, N. B., Mishra, A., Sutherland, B. A., O'Farrell, F. M., Buchan, A. M., Lauritzen, M., & Atwell, D. (2014). Capillary pericytes regulate cerebral blood flow in health and disease. *Nature*, 508(7494), 55–60.
- Hennig, J., Kiviniemi, V., Riemenschneider, B., Barghoorn, A., Akin, B., Wang, F., & LeVan, P. (2021). 15 years MR-encephalography. *Magnetic Resonance Materials in Physics, Biology and Medicine*, 34(1), 85–108.
- Hugger, T., Zahneisen, B., LeVan, P., Lee, K. J., Lee, H. L., Zaitsev, M., & Hennig, J. (2011). Fast undersampled functional magnetic resonance imaging using nonlinear regularized parallel image reconstruction. *PLoS One*, 6(12), e28822.
- Huotari, N., Raitamaa, L., Helakari, H., Kananen, J., Raatikainen, V., Rasila, A., Tuovinen, T., Kantola, J., Borchardt, V., Kiviniemi, V., & Korhonen, V. (2019). Sampling rate effects on resting state fMRI metrics. *Frontiers in Neuroscience*, 13, 279. <https://doi.org/10.3389/fnins.2019.00279>
- Hussein, A., Matthews, J. L., Syme, C., Macgowan, C., MacIntosh, B. J., Shirzadi, Z., Pausova, Z., Paus, T., & Chen, J. J. (2020). The association between resting-state functional magnetic resonance imaging and aortic pulse-wave velocity in healthy adults. *Human Brain Mapping*, 41(8), 2121–2135.
- Illiff, J. J., Wang, M., Zeppenfeld, D. M., Venkataraman, A., Plog, B. A., Liao, Y., Deane, R., & Nedergaard, M. (2013). Cerebral arterial pulsation drives paravascular CSF: interstitial fluid exchange in the murine brain. *The Journal of Neuroscience*, 33(46), 18190–18199.
- Jahani, H., Ni, W. W., Christen, T., Moseley, M. E., Tamura, M. K., & Zaharchuk, G. (2014). Spontaneous BOLD signal fluctuations in young healthy subjects and elderly patients with chronic kidney disease. *PLoS One*, 9(3), e92539.
- Jenkinson, M., Beckmann, C. F., Behrens, T. E. J., Woolrich, M. W., & Smith, S. M. (2012). FSL. *Neuroimage*, 62(2), 782–790.
- Kananen, J., Helakari, H., Korhonen, V., Huotari, N., Järvelä, M., Raitamaa, L., Raatikainen, V., Rajna, Z., Tuovinen, T., Nedergaard, M., Jacobs, J., LeVan, P., Ansakorpi, A., & Kiviniemi, V. (2020). Respiratory-related brain pulsations are increased in epilepsy: A two-center functional MRI study. *Brain Communication*, 2(2), fcaa076.
- Kananen, J., Tuovinen, T., Ansakorpi, H., Ryttyk, S., Helakari, H., Huotari, H., Raitamaa, L., Raatikainen, V., Rasila, A., Borchardt, V., Korhonen, V., LeVan, P., Nedergaard, M., & Kiviniemi, V. (2018). Altered physiological brain variation in drug-resistant epilepsy. *Brain and Behavior: A Cognitive Neuroscience Perspective*, 8(9), e01090.
- Khalil, A. A., Ostwaldt, A. C., Nierhaus, T., Ganeshan, R., Audebert, H. J., Villringer, K., Villringer, A., & Fiedbach, J. B. (2017). Relationship between changes in the temporal dynamics of the blood-oxygen-level-dependent signal and hypoperfusion in acute ischaemic stroke. *Stroke*, 48(4), 925–931.
- Kiviniemi, V., Wang, X., Korhonen, V., Keinänen, T., Tuovinen, T., Autio, J., LeVan, P., Keilholz, S., Zang, Y. F., Hennig, J., & Nedergaard, M. (2016). Ultra-fast magnetic resonance encephalography of physiological brain activity - Glymphatic pulsation mechanisms? *Journal of Cerebral Blood Flow and Metabolism*, 36(6), 1033–1045.
- Kuitunen, H., Tokola, S., Siniluoto, T., Isokangas, M., Sonkajärvi, E., Alahuhta, S., Turpeenniemi-Hujanen, T., Jantunen, E., Nousiainen, T., Vasala, K., & Kuitinen, O. (2017). Promising treatment results with blood brain barrier disruption (BBBD) based immunochemotherapy combined with autologous stem cell transplantation (ASCT) in patients with primary central nervous system lymphoma (PCNSL). *Journal of Neuro-Oncology*, 131(2), 293–300.
- Küker, W., Nägele, T., Korfel, A., Heckl, S., Thiel, E., Bamberg, M., Weller, M., & Herrlinger, U. (2005). Primary central nervous system lymphomas (PCNSL): MRI features at presentation in 100 patients. *Journal of Neuro-Oncology*, 72(2), 169–177.
- Lin, X., Khan, I. R. A., Seet, Y. H. C., Lee, H. Y., & Yu, W. (2020). Atypical radiological findings of primary central nervous system lymphoma. *Neuroradiology*, 62(6), 669–676.
- Liu, D., Liu, X., Ba, Z., Xie, L., Han, J., Yu, D., & Ma, X. (2019). Delayed contrast enhancement in magnetic resonance imaging and vascular morphology of primary diffuse large B-cell lymphoma (DLBCL) of the central nervous system (CNS): A retrospective study. *Medical Science Monitor*, 25, 3321–3328.
- Lohmann, G., Stelzer, J., Lacosse, E., Kumar, V. J., Mueller, K., Kuehn, E., Grodd, W., & Scheffler, K. (2018). LISA improves statistical analysis for fMRI. *Nature Communications*, 9(1), 4014.
- Makedonov, I., Black, S. E., & MacIntosh, B. J. (2013). BOLD fMRI in the white matter as a marker of aging and small vessel disease. *PLoS One*, 8(7), e67652.
- Makedonov, I., Chen, J. J., Masellis, M., MacIntosh, B. J., & Alzheimer's Disease Neuroimaging Initiative. (2016). Physiological fluctuations in white matter are increased in Alzheimer's disease and correlate with neuroimaging and cognitive biomarkers. *Neurobiology of Aging*, 37, 12–18.
- Mansour, A., Qandeel, M., Abdel-Razeq, H., & Abu-Ali, H. A. (2014). MR imaging features of intracranial primary CNS lymphoma in immune competent patients. *Cancer Imaging*, 14(1), 22.
- Meng, Y., Pople, C. B., Lea-Banks, H., Abrahao, A., Davidson, B., Suppiah, S., Vecchio, L. M., Samuel, N., Mahmud, F., Hynynen, K., Hamani, C., & Lipsman, N. (2019). Safety and efficacy of focused ultrasound induced blood-brain barrier opening: an integrative review of animal and human studies. *Journal of Controlled Release*, 309, 25–36.
- Mestre, H., Tithof, J., Du, T., Song, W., Peng, W., Sweeney, A. M., Olveda, G., Thomas, J. H., Nedergaard, M., & Kelley, D. H. (2018). Flow of cerebrospinal fluid is driven by arterial pulsations and is reduced in hypertension. *Nature Communications*, 9(1), 4878.
- Molnár, P. P., O'Neill, B. P., Scheithauer, B. W., & Groothuis, D. R. (1999). The blood-brain barrier in primary CNS lymphomas: Ultrastructural evidence of endothelial cell death. *Neuro-Oncology*, 1(2), 89–100.
- Niparuck, P., Boonsakan, P., Sutthipongkiat, T., Pukiat, S., Chanrathammachart, P., Phusanti, S., Boonyawat, K., Puavilai, T., Angchaisuksiri, P., Ungkanont, A., Chuncharunee, S., & Atichartakarn, V. (2019). Treatment outcome and prognostic factors in PCNSL. *Diagnostic Pathology*, 14(1), 56.

- O'Connor, T., Zhou, X., Kosla, J., Adili, A., Beccaria, M. G., Kotsiliti, E., Pfister, D., Johlke, A. L., Sinha, A., Sankowski, R., Schick, M., Lewis, R., Dokalis, N., Seubert, B., Höchst, B., Inverso, D., Heide, D., Zhang, W., Weihrich, P., ... Heikenwalder, M. (2019). Age-related gliosis promotes central nervous system lymphoma through CCL19-mediated tumor cell retention. *Cancer Cell*, 36(3), 250–267.
- Ogawa, S., Tank, D. W., Menon, R., Ellermann, J. M., Kim, S. G., Merkle, H., & Ugurbil, K. (1992). Intrinsic signal changes accompanying sensory stimulation: Functional brain mapping with magnetic resonance imaging. *Proceedings of the National Academy of Sciences of the United States of America*, 89(13), 5951–5955.
- Posse, S., Ackley, E., Mutihac, R., Zhang, T., Hummatov, R., Akhtari, M., Chohan, M., Fisch, B., & Yonas, H. (2013). High-speed real-time resting-state fMRI using multi-slab echo-volumar imaging. *Frontiers in Human Neuroscience*, 7, 479.
- Power, J. D., Mitra, A., Laumann, T. O., Snyder, A. Z., Schlaggar, B. L., & Petersen, S. E. (2014). Methods to detect, characterize, and remove motion artifact in resting state fMRI. *NeuroImage*, 84, 320–341.
- Raitamaa, L., Huotari, N., Korhonen, V., Helakari, H., Koivula, A., Kananen, J., & Kiviniemi, V. (2021). Spectral analysis of physiological brain pulsations affecting the BOLD signal. *Human Brain Mapping*, 42(13), 4298–4313.
- Rajna, Z., Mattila, H., Huotari, N., Tuovinen, T., Krüger, J., Holst, S. C., Korhonen, V., Remes, A. M., Seppänen, T., Hennig, J., Nedergaard, M., & Kiviniemi, V. (2021). Cardiovascular brain impulses in Alzheimer's disease. *Brain*, 144(7), 2214–2226.
- Rasmussen, M. K., Mestre, H., & Nedergaard, M. (2018). The glymphatic pathway in neurological disorders. *Lancet Neurology*, 17(11), 1016–1024.
- Sugita, Y., Terasaki, M., Nakashima, S., Ohshima, K., Morioka, M., & Abe, H. (2015). The perivascular microenvironment in primary central nervous system lymphomas: The role of chemokines and the endothelin B receptor. *Brain Tumor Pathology*, 32(1), 41–48.
- Tuovinen, T., Kananen, J., Rajna, Z., Lieslehto, J., Korhonen, V., Rytty, R., Mattila, H., Huotari, N., Raitamaa, L., Helakari, H., Elseoud, A. A., Krüger, J., LeVan, P., Tervonen, O., Hennig, J., Remes, A. M., Nedergaard, M., & Kiviniemi, V. (2020). The variability of functional MRI brain signal increases in Alzheimer's disease at cardiorespiratory frequencies. *Scientific Reports*, 10(1), 21559.
- Wise, R. G., Ide, K., Poulin, M. J., & Tracey, I. (2004). Resting fluctuations in arterial carbon dioxide induce significant low frequency variations in BOLD signal. *NeuroImage*, 21(4), 1652–1664.
- Xing, Z., You, R. X., Li, J., Liu, Y., & Cao, D. R. (2014). Differentiation of primary central nervous system lymphomas from high-grade gliomas by rCBV and percentage of signal intensity recovery derived from dynamic susceptibility-weighted contrast-enhanced perfusion MR imaging. *Clinical Neuroradiology*, 24(4), 329–336.

SUPPORTING INFORMATION

Additional supporting information may be found in the online version of the article at the publisher's website.

How to cite this article: Poltojaime, V., Kemppainen, J., Keinänen, N., Bode, M., Isokangas, J.-M., Kuitunen, H., Nikkinen, J., Sonkajärvi, E., Korhonen, V., Tuovinen, T., Järvelä, M., Huotari, N., Raitamaa, L., Kananen, J., Korhonen, T., Tetri, S., Kuittinen, O., & Kiviniemi, V. (2022). Physiological instability is linked to mortality in primary central nervous system lymphoma: A case-control fMRI study. *Human Brain Mapping*, 43(13), 4030–4044. <https://doi.org/10.1002/hbm.25901>